The Positive-Parity Baryon Spectrum and the Role of Hybrid Baryons

Tanjib Khan[1], David Richards[2], Frank Winter[2]
[1] *Department of Physics, The College of William and Mary, Williamsburg, Virginia, USA.*
[2] *Thomas Jefferson National Accelerator Facility, Newport News, Virginia, USA.*

We calculate the low-lying spectra for the positive-parity Δ and N at two pion masses of 358 and 278 MeV using an isotropic clover action with two degenerate light-quark and one strange-quark flavors through the application of the generalized variational method within the distillation framework. The spectrum exhibits the general feature observed in previous calculations using an anistropic clover lattice, with a counting of states at least as rich as the quark model. Furthermore, we identify states that are hybrid in nature, where gluonic degrees of freedom play a structural role, indicating that such states appear a feature of the excited baryon spectrum, irrespective of the lattice action, or the precise details of the smearing of the lattice interpolating operators used to identify such states.

I. INTRODUCTION

Lattice QCD (LQCD) provides a powerful numerical approach to solve QCD from the first principles, and has been successfully applied to address a range of key quantities in high-energy and nuclear physics, from the calculation of the ground-state spectrum, to nuclear charges and measure of hadron structure. The calculation of the excited-state spectrum of QCD presented a particular challenge, in that the formulation of lattice QCD in Euclidean space precluded the direct calculation of scattering amplitudes. However, the realization that the energy shifts at finite volume could be related to infinite-volume scattering amplitudes [1], has transformed our ability to study the resonance spectrum and the interaction of hadrons from lattice QCD. There has been impressive progress at applying these methods to our understanding of the meson spectrum [2–6], but their application to the study of the baryon spectrum [7], where both the theoretical and computational challenges are more demanding, is somewhat limited.

Most studies of the excited-baryon spectrum have interpreted the extracted energy levels as those of single-particle, stable states, with only a few attempts at extracting the momentum-dependent scattering amplitude [8–10] and thereby correctly treating the resonance spectrum. However, accepting this important limitation, considerable insight into the excited baryon spectrum of QCD has been obtained. Most notably, the extracted spectrum is found to be at least as rich as the quark model, and exhibits a counting of energy levels commensurate with $\mathrm{SU}(6) \otimes \mathrm{O}(3)$ spin-flavor symmetry [11]. Moreover, the positive-parity excited baryon spectrum reveals suggestions of "hybrid" states, that is those in which the gluonic degrees of freedom play an essential, structural role, beyond those of the quark model, with a common mechanism with comparable states in the meson section [12]. For the case of mesons, there can exist "exotic" states that have quantum numbers J^{PC} not available within a regular $q\bar{q}$ valence structure. Such states may have a dominant $qq\bar{q}\bar{q}$ component, so-called tetraquarks [13, 14], or be predominantly "hybrid" $q\bar{q}g$ states [15–19], with a manifest gluonic valence component. Thus it is straightforward to separate an "exotic" meson state from a regular one. But for baryons, the regular qqq states can have all the J^P values. So, hybrid or so-called pentaquark states will always have to "share" quantum numbers with regular states, thus making them very difficult to study.

There has been a number of models proposed to calculate the spectrum of hybrid baryons. There is the bag model [20] where quark and gluon fields are confined within a cavity with the fields satisfying appropriate boundary conditions at the wall of the cavity. In the flux-tube model [21, 22], the quarks sit at the ends of a string-like structure. A meson contains a single flux tube between the quark and the anti-quark; in a hybrid meson, this string is excited by a transverse oscillation. For the case of a baryon, there are three tubes which either meet at a junction or form a triangle. There are also QCD sum-rule methods [23] and quark potential models [24] that make predictions about hybrid baryons.

For the case of the so-called "hybrid" baryons, and indeed for the non-exotic hybrids catalogued from lattice calculations in the meson sector [25], their identification has proceeded through observing that the dominant interpolating operators are "hybrid" in nature, in the sense that the operators vanish for trivial unit gauge configurations. Such an identification, by its nature introduces a degree of model dependence, and therefore it is important to study the robustness of such an identification. The aim of this paper is precisely to test such robustness by performing a calculation of the low-lying positive-parity baryon spectrum at pion masses lower than those of ref. [12], using different gauge and fermion actions at a finer spatial lattice spacing.

The remainder of the paper is organized as follows. In section II, we describe the baryon interpolation operators used in our calculation, and briefly outline the distillation methodology used to construct the correlation functions and our implementation of the variational method. Section III contains our results, beginning with the parameters of the ensembles used in the calculation, a description of our fitting procedure, the stability of the fits under the variation of the parameters of distillation process and the robustness of the spin identification on our lattices, before presenting our analysis of the low-lying positive-parity Δ and N spectrum together with the quark-gluon assignment of the states, followed by the identification of the hybrid baryons for both the Δ and N. In section IV, we summarize our work and outline some implications.

II. COMPUTATIONAL STRATEGY

Since the focus of our calculation is the low-lying positive-parity spectrum, we employ a basis of interpolating operators that have been found to have dominant overlaps with those states. The construction of the interpolating operators, and the identification of the operators that couple primarily to the low-lying spectrum, has been described in detail in refs. [11] and [12], so we only summarize the salient elements here. The interpolating operators follow a continuum construction, and are expressed as a product of terms describing the flavor structure, Dirac spin and

J	irrep. (dimension)	No. of Ops (Δ)	No. of Ops (N)
$\frac{1}{2}$	$G_1(2)$	3 (1)	7 (2)
$\frac{3}{2}$	$H(4)$	5 (1)	7 (2)
$\frac{5}{2}$	$G_2(2) \oplus H(4)$	2 + 2	4 + 4 (1 + 1)
$\frac{7}{2}$	$G_1(2) \oplus G_2(2) \oplus H(4)$	1 + 1 + 1	1 + 1 + 1

TABLE I. The numbers of Δ and N interpolating operators used in the calculation, together with their subductions onto the irreps. of the cubic group. The number of hybrid operators used in each irrep. is included within bracket.

orbital angular momentum implemented through derivatives:

$$\left(\mathrm{B}_{\Sigma_\mathrm{F}} \otimes \left(\mathrm{S}^{\mathrm{P_S}}\right)^{n}_{\Sigma_\mathrm{S}} \otimes \mathrm{D}^{[d]}_{\mathrm{L},\,\Sigma_\mathrm{D}}\right)^{\mathrm{J}}$$

where B, S and D denote the flavor, Dirac spin and orbital angular momentum, L, components respectively, and $\Sigma_F, \Sigma_S, \Sigma_D$ are the corresponding permutation symmetries. The resulting operators are projected through suitable Clebsch-Gordon coefficients to total spin J; the label n distinguishes different combinations that have the same spin structure, while the d is the order of the gauge-covariant derivative.

For this work, our basis comprises the non-relativistic operators constructed from the upper components, in a suitable γ representation of the Dirac spinors, with up to two covariant derivatives, allowing the operators with up to two units of orbital angular momenta. We also include additional operators containing the commutator of two covariant derivatives acting on the same quark field, corresponding to the chromomagetic components of the gluonic field-strength tensor; it is these operators, which vanish for a unit gauge configuration, that are referred to as "hybrid" operators, and for which a dominant overlap with a given state, we treat as the signature of the hybrid nature of that state, as we discuss below. Finally, as the calculations are done on a discretized lattice, the operators are subduced from the continuous Hilbert space onto the different lattice irreps. As a consequence, for total angular momentum $J = \frac{5}{2}$ and higher, the continuum operators are subduced onto multiple irreps, as detailed in Table I.

The operators created directly from the fields of the lattice Lagrangian couple to states at all scales, thus making the extraction of the lightest states in the spectrum difficult. In order to solve this problem, a linear operator is applied on the quark fields on appropriate time-slices and operators are built from those "smeared" fields. In this work, the smearing method used is known as Distillation [26]. The distillation operator is defined as:

$$\Box_{xy}(t) = \sum_{k=1}^{N_D} \nu_x^{(k)}(t)\, \nu_y^{(k)\dagger}(t) \quad \Rightarrow \quad \Box(t) \equiv V_D(t)\, V_D^\dagger(t) \tag{1}$$

where $V_D(t)$ is a $M \times N_D$ matrix, $M = N_c \times N_x \times N_y \times N_z$, N_c is the number of colors, N_x, N_y, N_z are the extents of the lattice in the three spatial directions. The k^{th} column of $V_D(t)$, $\nu_x^{(k)}(t)$ is the k^{th} eigenvector of the second-order three-dimensional differential operator $\bigtriangledown^2$ evaluated on the background of the spatial gauge fields of time-slice t, once the eigenvectors have been sorted by the ascending order of the eigenvalues; N_D is the dimension of the distillation space. The reasons for adopting distillation in our calculation are, firstly, that the computationally demanding parallel transporters of the theory, the perambulators, depend only on the gauge field, and not on the interpolating operators. So, we can calculate the perambulators on an ensemble of gauge field once, and then reuse them for an arbitrary basis of operators at both the source and the sink, and indeed for a range of calculations. Secondly, the low-energy component of the spectrum is faithfully captured with a relatively small number of distillation vectors, as we investigate in the next section.

For the extraction of the spectrum and the associated overlaps, we use the variational method as implemented in ref. [27]. Our starting point is the generalized eigenvalue equation (GEV) for the two-point correlator matrix $C(t)$ with elements

$$C_{ij}(t) = \langle 0 \mid O_i(t) \bar{O}_j(0) \mid 0 \rangle \tag{2}$$

where without loss of generality we take the source interpolation operator to be at time slice $t = 0$, and where i, j

ID	a (fm)	M_π (MeV)	$L^3 \times N_t$	$N_{\rm cfg}$
$a94m358$	0.094(1)	358(3)	$32^3 \times 64$	351
$a94m278$	0.094(1)	278(4)	$32^3 \times 64$	259

TABLE II. The parameters of the lattices, where the scale is obtained using w_0 [30], and $N_{\rm cfg}$ is the number of configurations.

label the operators in a given representation of the cubic group. The GEV equation is expressed as

$$C(t)\ u_\alpha = \lambda_\alpha(t,t_0)\ C(t_0)\ u_\alpha \tag{3}$$

where u_α are the generalized eigenvectors satisfying the orthonormality condition $u_\alpha^\dagger\ C(t_0)\ u_\beta = \delta_{\alpha\beta}$, and $\lambda_\alpha(t,t_0)$ are the corresponding principle correlators behaving as

$$\lambda_\alpha(t,t_0) = e^{-m_\alpha(t-t_0)}\Big[1+\mathcal{O}\big(e^{-\delta m(t-t_0)}\big)\Big] \tag{4}$$

Here m_α is the energy of the state labeled by α and δm represents the contributions from other states. Our subsequent results are derived from two-state fits to the principle correlators of this form. Furthermore, $C_{ij}(t)$ can be decomposed into the form,

$$C_{ij}(t) = \sum_\alpha \frac{Z_i^{\alpha^*}\ Z_j^\alpha}{2m_\alpha} e^{-m_\alpha t} \tag{5}$$

where, the overlap factor, $Z_i^\alpha = \langle 0|O_i|\alpha\rangle$ can be written as,

$$Z_i^\alpha = \big(U^{-1}\big)_i^\alpha\ \sqrt{2m_\alpha}\ \exp\!\left(\frac{m_\alpha t_0}{2}\right) \tag{6}$$

where the matrix U is formed using the generalized eigenvectors u_α as its columns; it satisfies the orthonormality condition, $U^\dagger C(t_0) U = I$. The overlaps can, thereby be obtained from the solution of the generalized eigenvector matrix.

III. RESULTS

A. Computational Details

Earlier calculations using this basis of operators were performed on anisotropic clover lattices, with a spatial lattice spacing of around $a \simeq 0.12$ fm, and an anisotropy, $\xi \equiv a_s/a_t \simeq 3.5$ [28, 29] with two mass-degenerate light-quark flavors and a strange-quark. Here we use an isotropic clover action at a smaller lattice spacing $a \simeq 0.094$ fm, determined using w_0 scale [30], and with $2+1$ flavors. We use ensembles at two values of the light-quark masses, corresponding to pion masses of $m_\pi = 358$ and 278 MeV respectively. Details of the parameters of our ensemble are listed in Table II. All the gauge-links entering in the operator constructions are stout-smeared [31]. In order to achieve the greatest sampling of the lattice, we evaluate the two-point correlators from each time-slice on the lattice, and on each configuration, average the correlators over lattice time-slices to remove the correlations among the temporal direction of the lattices. We compute the perambulators for $N_D = 64$ eigenvectors. We use positive parity operators from [12] for the Δ (Isospin, $I = \frac{3}{2}$, $I_z = +\frac{3}{2}$) and for the N (Isospin, $I = \frac{1}{2}$, $I_z = +\frac{1}{2}$).

B. Fitting Procedure

The fitting procedure of the two-point correlators with respect to the lattice time to extract the mass spectra and the overlap factors, is defined in detail in ref. [16], and we only summarize the details here. The GEV of eqn. 2 is solved over a range of t_0, and for each t_0, the resulting principle correlators are fit to the two-exponential form,

$$\lambda_\alpha(t,t_0) = (1-A)e^{-m_\alpha(t-t_0)} + Ae^{-m'_\alpha(t-t_0)}. \tag{7}$$

We restrict the fitting range such that, for each principle correlator, we only include time-slices for which the noise-to-signal ratio is less than 0.05; in practice, this restricts the largest value of t included in the fits to be around 8. Furthermore, in the fits, we only include the two-point correlators with source-sink separation greater than 2 lattice units in temporal direction to avoid possible contact terms. For each t_0, our fit to each principle correlator is based on an acceptable χ^2/dof. We also require that the coefficient A in eqn. 7 is far less than one, such that for a fit to an N-dimensional matrix of correlators, the matrix is largely saturated by the lowest-lying N states. As m'_α of eqn. 7 is another measure of the excited-state contribution to the fit, we require m'_α to be less than 10% of the parameter m_α which we identify as the mass of the corresponding state. Finally, we compute the overlap factors of eqn. 6 using the eigenvectors at a reference time-slice t_z.

In Figure 1, we show the principal correlator fit for the H_g irrep. of the Δ. A simultaneous fit is done for all the operators used for this irrep. Each box shows the fit results for a particular state where the continuous curve is the reconstruction from the fitted parameters and the purple region indicates the data points which are included in the fit. As we keep A and m'_α as small as possible, the curve in each box falls exponentially for smaller lattice time-slice and flattens out to unity for $t > t_0$. The box at the top-left corner shows the fit for the ground state which is determined very preciously with very small uncertainty in mass. As we go to higher and higher excited states, the uncertainty of mass increases in general. The highest excited state for this fit is shown in the bottom-middle box where the uncertainty of the mass is visible in the plot.

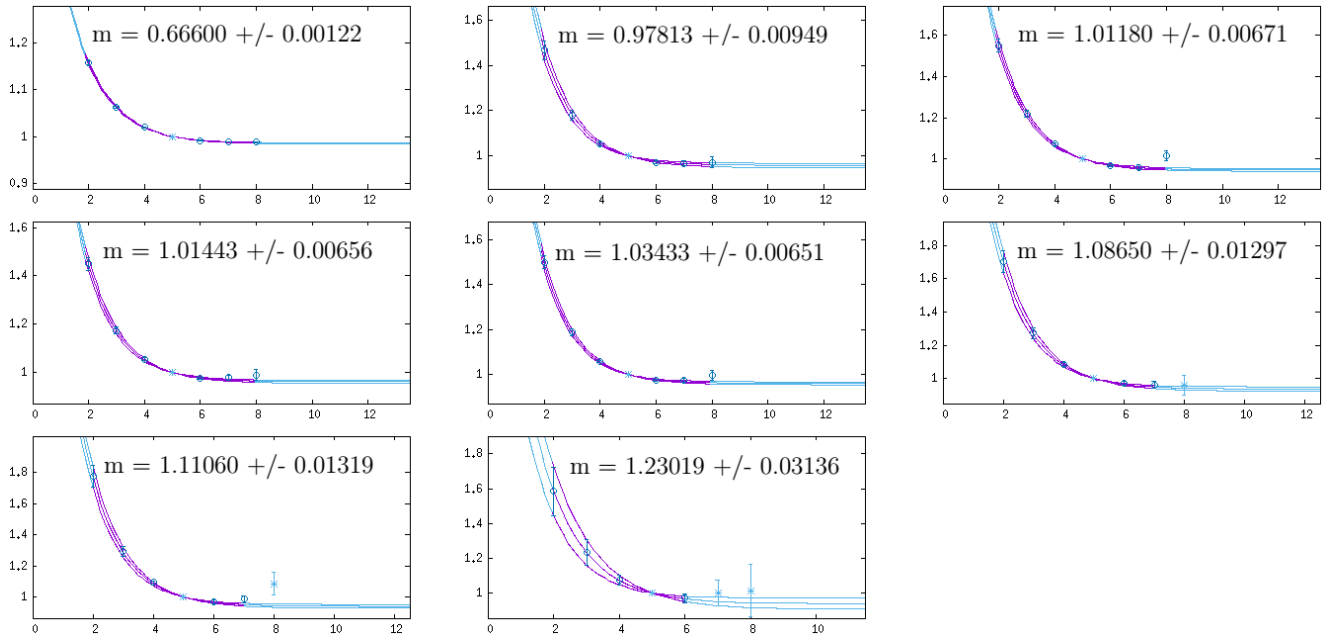

FIG. 1. Principal correlator fit for the low-lying positive-parity spectrum of H_g irrep. of the Δ for $t_0 = 5$ on lattice $a94m358$. The plot shows $\lambda_\alpha(t, t_0).e^{m_\alpha(t-t_0)}$ data on the y-axes and the lattice time-slices on the x-axes. In each box, the mass of the state is labelled by m.

C. Stability under variation of Distillation Space

The expectation is that rank N_D of the distillation space should scale as the physical spatial volume of the lattice in order to maintain the same low-energy physics. Previous studies of the low-lying baryon spectrum on a lattice of 16^3 spatial volume at a lattice spacing $a \simeq 0.12$ fm employed $N_D = 56$ distillation eigenvectors, suggesting that as many as 230 eigenvectors might be needed to capture the same physics of our lattice. The cost of computing the two-point functions of eqn 2 scales as N_D^4, and thus there is a computational demand to use as small a basis of eigenvectors as possible whilst still capturing the essential physics. In this paper, we have generated perambulators and the baryon elementals that encode the operators for $N_D = 64$ eigenvectors, and begin our discussion by examining the sensitivity of the extracted spectra to the variation of N_D. In Figure 2, we show the lowest energy levels in the positive-parity H_g irreducible representation of the Δ as we reduce the number of eigenvectors down to $N_D = 24$. While the ground state is indeed reliably extracted with only a minimal number of eigenvectors, it is only when we reach $N_D = 56$ eigenvectors that the lowest five states are obtained with acceptable uncertainties, with

consistency between the $N_D = 56$ and $N_D = 64$ determinations. We will therefore use $N_D = 64$ in the remaining discussion.

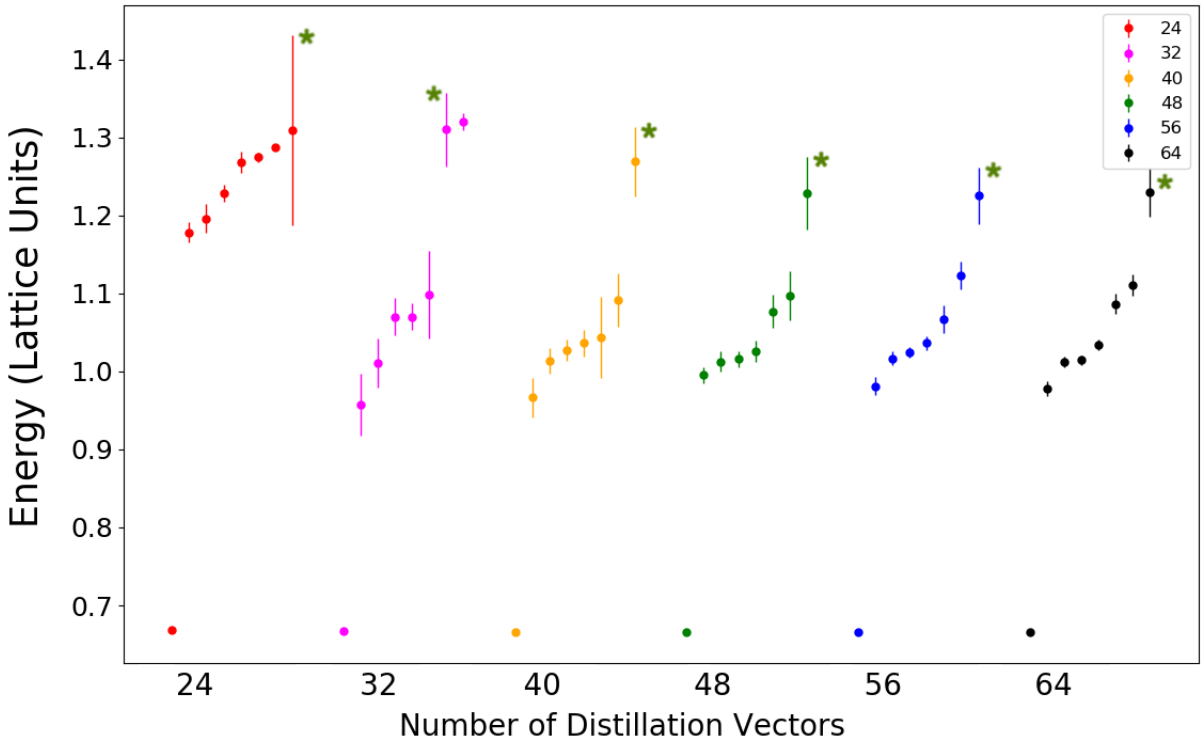

FIG. 2. The dependence of the Δ spectrum in the H_g irrep. on the number of distillation vectors N_D for the ensemble $a94m358$ of Table II. The states we identify as hybrid baryons are indicated by green asterisks, as discussed in the text.

D. Spin Identification

The breaking of rotational symmetry induced by the discretization onto the lattice renders the determination of the spin corresponding to the different energy levels within the irreps. less than straightforward. In the case of the glueball spectrum in pure Yang-Mills theory [32], the identification of the spins was accomplished by the identification of degeneracies across different lattice irreps. in the approach to the continuum limit. This requires the generation of ensembles at several lattice spacings, a formidable task once quark degrees of freedom are included, and further requires statistical precision far beyond that attainable with reasonable computational cost to delineate overlapping energies within the spectrum. We need a spin identification method which uses data obtained from only a single lattice spacing, albeit one sufficiently fine that it preserves the rotational symmetry to a sufficient degree at the hadronic scale.

Here we use the method introduced in ref. [17], and applied for the baryon spectrum in refs. [11, 12] whereby the operator overlap factors are used to identify the spin of a state. It relies on the observation that each operator used in the calculation carries an essence of the continuum spin of the operator from which it is subduced, and therefore we would expect an operator subduced from, say angular momentum J, to have large overlaps only with states of the same continuum angular momentum J. Positive-parity states corresponding to the continuum angular momentum $J = \frac{5}{2}$ and $J = \frac{7}{2}$ will appear in the spectrum of the H_g and $G2_g$ irreps, and of the H_g, $G1_g$ and $G2_g$ irreps. respectively, and we would expect overlaps to be dominated by the operators subduced from the same continuum operators across those irreps. This is indeed what we observe, as can be seen in Figure 3 for the Δ spectrum, where the overlaps are obtained from a variational analysis using all the operators within a given lattice irrep. Further, we find the resulting energies are degenerate, with, for states of spin $\frac{5}{2}$ and $\frac{7}{2}$, the energies obtained in the H_g irrep. within 1% of the values obtained in the $G1_g$ and, for the case of spin $\frac{7}{2}$, $G2_g$ irreps.

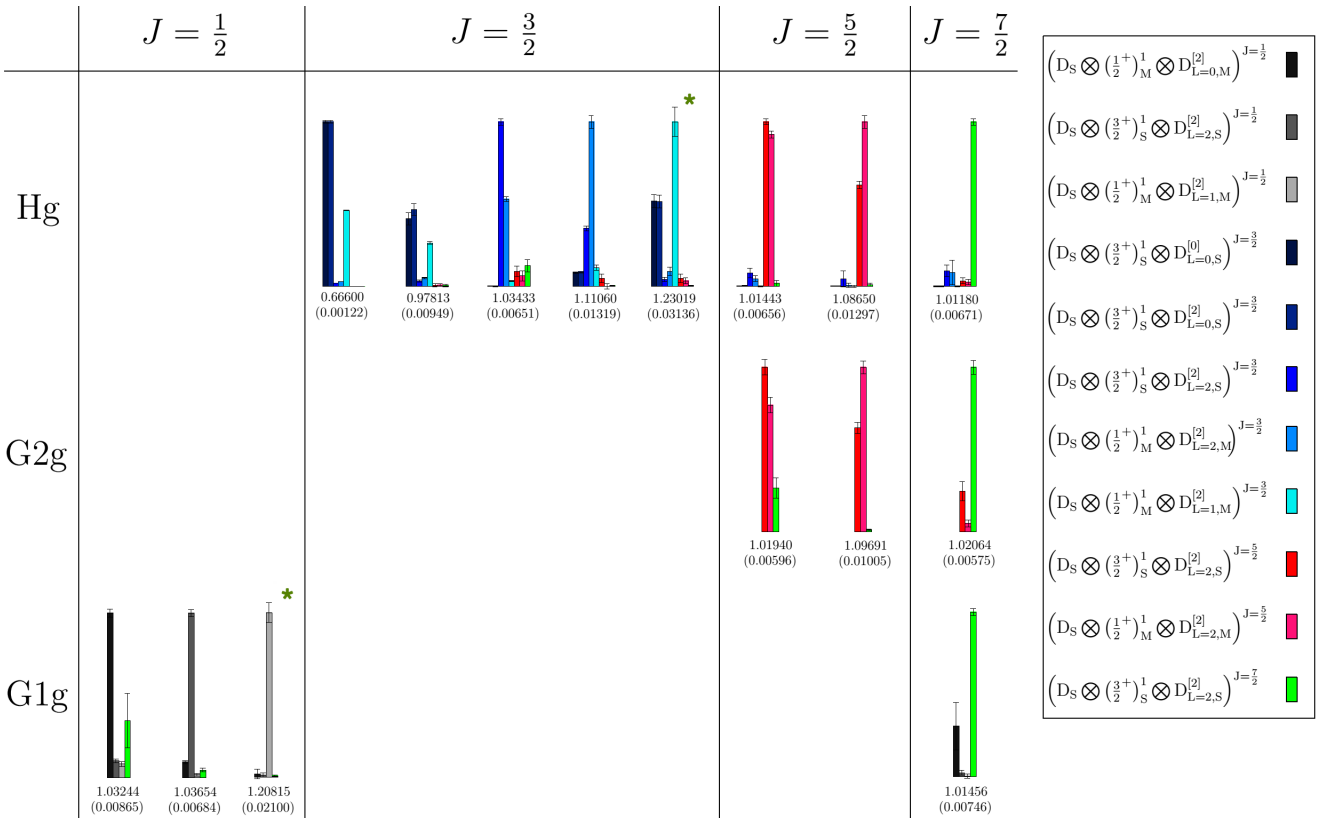

FIG. 3. Histogram plot of the operator overlaps Z for the Δ on the $a94m358$ ensemble, normalized such that, for a given operator, the largest overlap across all states is unity. The overlaps are obtained from a variational analysis across all operators within a given lattice irrep, irrespective of the continuum spins from which they are derived.

E. Delta & Nucleon Spectra

Having established the effectiveness of our spin-identification procedure, and the empirical decoupling of operators derived from different continuum spins, we now proceed as follows. Rather than applying the variational method to a basis comprising all the operators within a lattice irrep, we instead apply the method to a more restricted basis of operators comprising those operators within an irrep. derived from a given continuum J. In figure 4, the Δ spectrum obtained by analysing all the operators within a given lattice irrep. is compared with that where we apply the varational method in each lattice irrep. to only those operators derived from a given continuum spin. The comparison reveals that there are no significant differences between these two spectra, prompting us to analyse the operators of each angular momentum separately as this requires calculating the two-point correlators using a smaller basis of operators at one time; since the computational cost of computing the full correlation matrix goes as the square of the operator basis, this reduces the computational cost significantly.

The low-lying positive-parity spectra of the Δ and N for both the $a94m278$ and $a94m358$ ensembles using this fitting procedure are shown in Figures 5 and 6, respectively. For the spin $\frac{5}{2}$ and spin $\frac{7}{2}$ energy levels, the splittings between the values obtained in the H_g and $G2_g$, and in the H_g, $G2_g$ and $G1_g$ irreps, respectively, are remarkably small, reflecting the partial $\mathcal{O}(a^2)$ breaking of rotational symmetry, and the smaller spatial lattice spacing than that used in comparable studies using an anisotropic lattice. As expected, the quality of the spectrum is somewhat worse at the lighter value of the quark mass, and the spin identification procedure less convincing at the highest energies for the N particle. We emphasise that the qualitative properties of the spectrum, and in particular the counting of states, is consistent with that obtained on the anisotropic lattices at a coarse value of the spatial lattice spacing, but a considerably finer temporal lattice spacing.

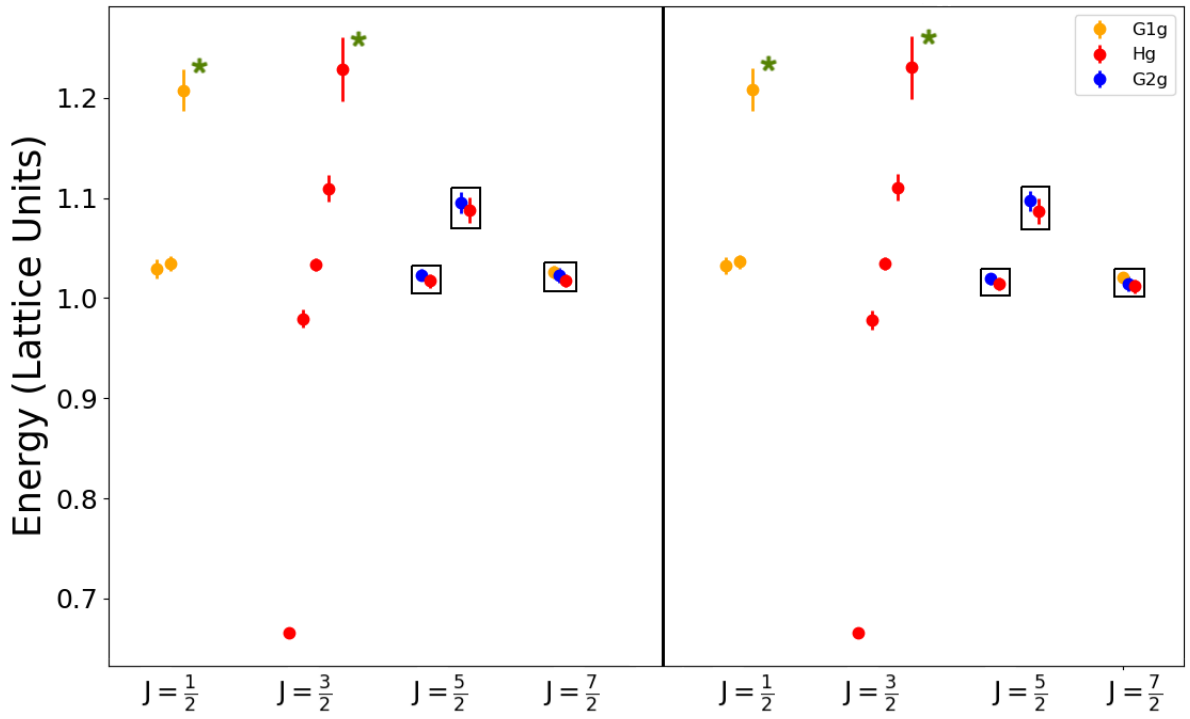

FIG. 4. Comparison of low-lying Δ spectra on the $a94m358$ ensemble between fitting with the operators subduced from the same angular momentum separately (left), and fitting with all the operators within a lattice irrep, irrespective of their continuum antecedents. For the states identified as spin $\frac{5}{2}$ and $\frac{7}{2}$, the boxes contain the energy levels obtained after the subduction onto the different lattice irreps. Energy levels identified as those of hybrid states are denoted by the green asterisks.

1. *Hybrid States*

As we noted in the introduction, in contrast to the case of the meson spectrum, "exotic" baryons cannot be distinguished through their quantum numbers. Therefore, the identification of baryons as "hybrid" in nature inevitably involves a degree of model dependence. Here we identify the hybrid states as those whose overlap, defined through eqn. 6, is predominantly with hybrid-type operators, that is those that would vanish for the case of a trivial gauge configuration [12]. For the case of the Δ, this identification is very apparent, as can be seen in Figure 3 for the ensemble at heavier pion mass, where we find one hybrid state in the $J = \frac{1}{2}$ channel and one in $J = \frac{3}{2}$ channel. For the N spectrum on the heavier ensemble $a94m358$, we likewise find clear evidence for hybrid-baryon states through the nature of their overlaps, where we identify two states in the $J = \frac{1}{2}$ channel, two states in the $J = \frac{3}{2}$ channel and one state in the $J = \frac{5}{2}$ channel. On the lighter $a94m278$ ensemble, the identification and multiplicities of hybrid baryons for the channels $J = \frac{3}{2}$ & $J = \frac{5}{2}$ follows those on the heavier ensemble. However, for the $J = \frac{1}{2}$ channel, there is no obvious candidate for a hybrid baryon using the criterion of the operator overlap. In spite of this, the multiplicity in both the Δ and N spectrum confirm the findings in the earlier studies using the anisotropic lattice [12], with a multiplicity of states at least as rich as the quark model, and the presence of additional states that appear to be hybrid in nature.

IV. CONCLUSIONS

In this work, we have computed the positive-parity Δ and N spectra using an isotropic clover action. Our results support the observations in earlier works at heavier pion masses, and using the anisotropic clover action at a coarser spatial lattice spacing, but finer temporal lattice spacing. In particular, we find that rotational symmetry is largely observed at the hadronic scale, enabling us to reliably identify the spins of the states through their predominant overlap onto operators derived from continuum operators of definite spin. Furthermore, we find that the low-lying spectrum can be determined using a somewhat modest number of eigenvectors without the use of a stochastic variant, indicating that distillation does indeed form an effective framework for the study of baryons.

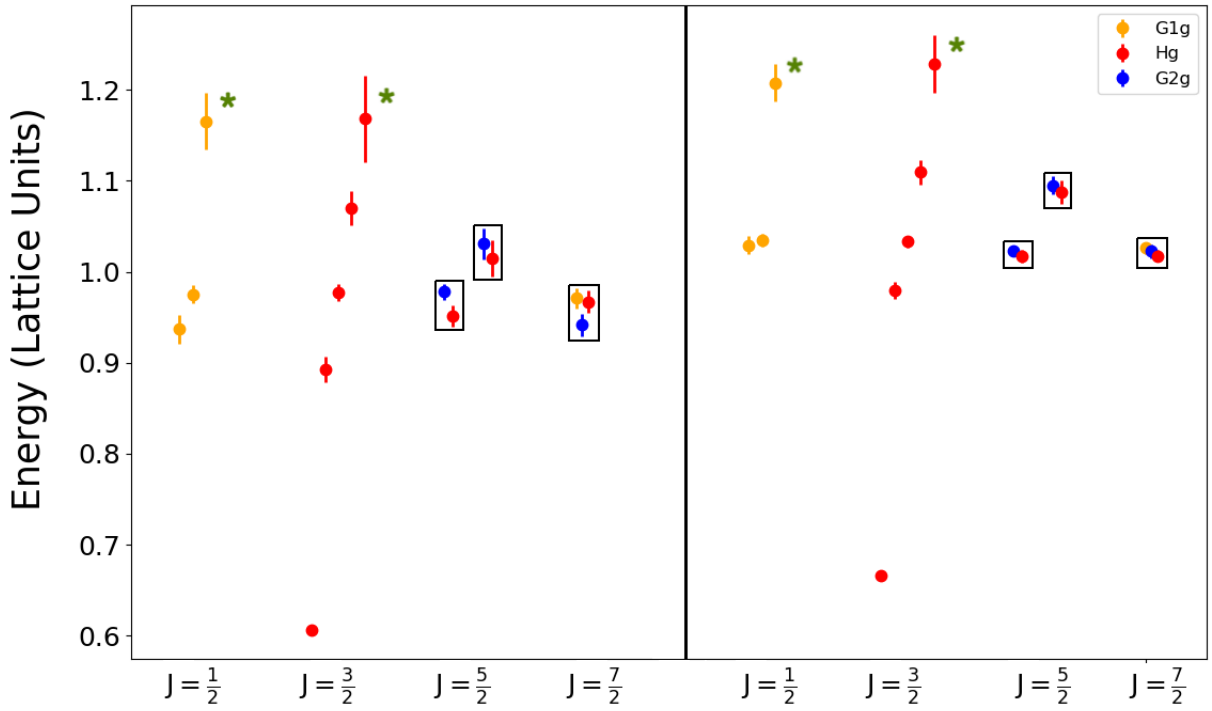

FIG. 5. The low-lying positive-parity Δ spectrum in lattice units on the $a94m278$ (left) and $a94m358$ (right) ensembles, using the fitting procedure described in the text. For the states identified as spin $\frac{5}{2}$ and $\frac{7}{2}$, the boxes contain the energy levels obtained after the subduction onto the different lattice irreps. Energy levels identified as those of hybrid states are denoted by the green asterisks.

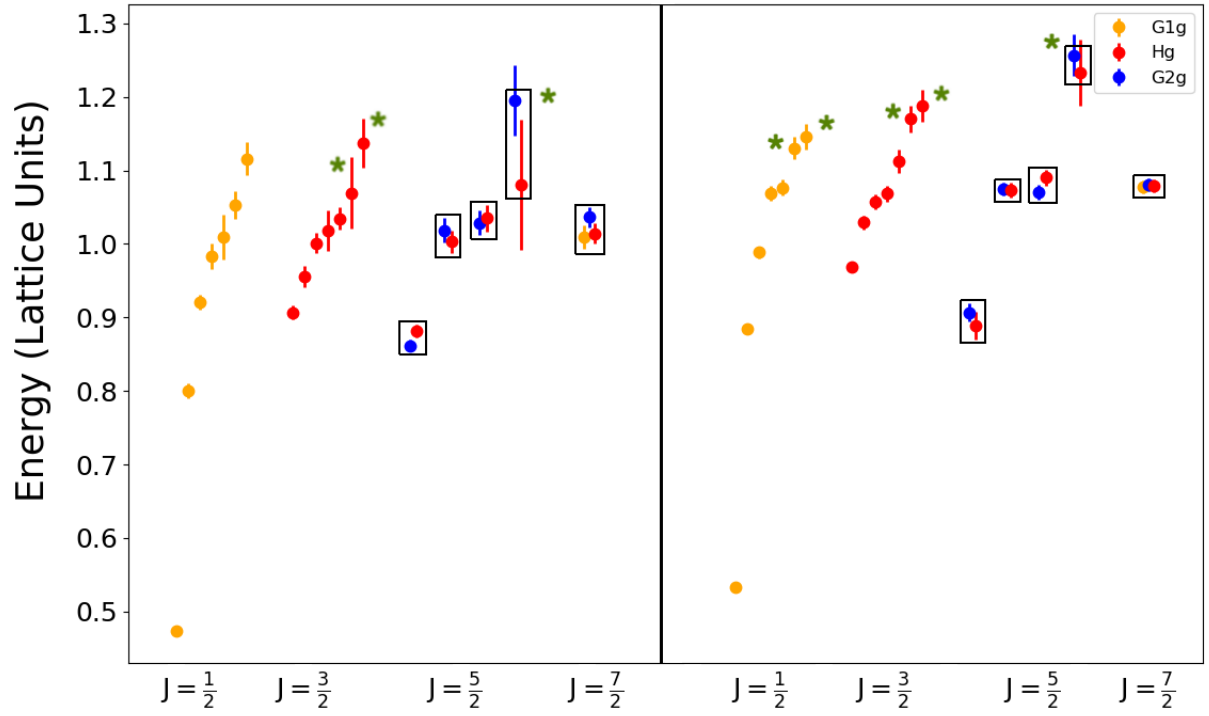

FIG. 6. The low-lying positive-parity N spectrum in lattice units on the $a94m278$ (left) and $a94m358$ (right) ensembles, using the fitting procedure described in the text. For the states identified as spin $\frac{5}{2}$ and $\frac{7}{2}$, the boxes contain the energy levels obtained after the subduction onto the different lattice irreps. Energy levels identified as those of hybrid states are denoted by the green asterisks.

However, the most significant outcome of this work is that we find that the spectra exhibit a counting of states in line with that of the quark model, but with additional states that we can identify as "hybrid" in nature, with the gluonic degrees of freedom playing a structural role. This work has important limitations in each use of "single-hadron" operators, and the treatment of states as discrete energies in the spectrum with no attempt to extract the momentum-dependent phase shifts. However, the observations are significant since the means to identify such hybrids through the predominant overlap of a class of "hybrid" operators, pioneered in ref. [12], must inevitably raise the issue of the operator-dependence of such an identification. Here we use a different action, with a different lattice spacing and essentially different interpolating operators implemented through the variation of the number of distillation eigenvectors. Thus the identification of hybrid-type states in the spectrum is indeed robust. Ultimately, a determination of the quark and gluon content of such resonances through the probing of their structure will be desired, and the theoretical framework for such studies is an area of rapid development [33–35].

V. ACKNOWLEDGMENTS

We thank Jozef Dudek, Robert Edwards, Archana Radhakrishnan and Christopher Johnson for useful discussions, and for the use of the `reconfit` fitting package. This work is supported by the U.S. Department of Energy, Office of Science, Office of Nuclear Physics under contract DE-AC05-06OR23177. Computations for this work were carried out in part on facilities of the USQCD Collaboration, which are funded by the Office of Science of the U.S. Department of Energy. This work was performed in part using computing facilities at The College of William and Mary which were provided by contributions from the National Science Foundation (MRI grant PHY-1626177), and the Commonwealth of Virginia Equipment Trust Fund. This work used the Extreme Science and Engineering Discovery Environment (XSEDE), which is supported by National Science Foundation grant number ACI-1548562. Specifically, it used the Bridges system, which is supported by NSF award number ACI-1445606, at the Pittsburgh Supercomputing Center (PSC) [36, 37]. In addition, this work used resources at NERSC, a DOE Office of Science User Facility supported by the Office of Science of the U.S. Department of Energy under Contract #DE-AC02-05CH11231, as well as resources of the Oak Ridge Leadership Computing Facility at the Oak Ridge National Laboratory, which is supported by the Office of Science of the U.S. Department of Energy under Contract No. #DE-AC05-00OR22725. The software codes `Chroma` [38], `QUDA` [39, 40] and `QPhiX` [41] were used in our work. The authors acknowledge support from the U.S. Department of Energy, Office of Science, Office of Advanced Scientific Computing Research and Office of Nuclear Physics, Scientific Discovery through Advanced Computing (SciDAC) program, and of the U.S. Department of Energy Exascale Computing Project. TK was support in part by the Center for Nuclear Femtography grants C2-2020-FEMT-006, C2019-FEMT-002-05.

[1] M. Luscher, Commun. Math. Phys. **104**, 177 (1986).
[2] D. J. Wilson, R. A. Briceno, J. J. Dudek, R. G. Edwards, and C. E. Thomas, Phys. Rev. D **92**, 094502 (2015), arXiv:1507.02599 [hep-ph].
[3] D. J. Wilson, J. J. Dudek, R. G. Edwards, and C. E. Thomas, Phys. Rev. D **91**, 054008 (2015), arXiv:1411.2004 [hep-ph].
[4] J. J. Dudek, R. G. Edwards, C. E. Thomas, and D. J. Wilson (for the Hadron Spectrum Collaboration), Phys. Rev. Lett. **113**, 182001 (2014).
[5] R. Brett, J. Bulava, J. Fallica, A. Hanlon, B. Hörz, and C. Morningstar, Nuclear Physics B **932**, 29 (2018).
[6] J. Bulava, B. Fahy, B. Hörz, K. J. Juge, C. Morningstar, and C. H. Wong, Nuclear Physics B **910**, 842 (2016).
[7] J. Bulava, R. G. Edwards, E. Engelson, B. Joó, H.-W. Lin, C. Morningstar, D. G. Richards, and S. J. Wallace (Hadron Spectrum Collaboration), Phys. Rev. D **82**, 014507 (2010).
[8] C. Morningstar, J. Bulava, B. Fahy, J. Foley, Y. C. Jhang, K. J. Juge, D. Lenkner, and C. H. Wong, Phys. Rev. D **88**, 014511 (2013).
[9] C. W. Andersen, J. Bulava, B. Hörz, and C. Morningstar, Phys. Rev. **D97**, 014506 (2018), arXiv:1710.01557 [hep-lat].
[10] C. Lang, L. Leskovec, M. Padmanath, and S. Prelovsek, Phys. Rev. D **95**, 014510 (2017), arXiv:1610.01422 [hep-lat].
[11] R. G. Edwards, J. J. Dudek, D. G. Richards, and S. J. Wallace, Phys. Rev. D **84**, 074508 (2011), arXiv:1104.5152 [hep-ph].
[12] J. J. Dudek and R. G. Edwards, Phys. Rev. D **85**, 054016 (2012), arXiv:1201.2349 [hep-ph].
[13] G. K. C. Cheung, C. E. Thomas, J. J. Dudek, and R. G. Edwards (Hadron Spectrum), JHEP **11**, 033 (2017), arXiv:1709.01417 [hep-lat].
[14] P. Junnarkar, N. Mathur, and M. Padmanath, Phys. Rev. D **99**, 034507 (2019), arXiv:1810.12285 [hep-lat].
[15] M. Chanowitz and S. Sharpe, Nuclear Physics B **222**, 211 (1983).
[16] J. J. Dudek, R. G. Edwards, M. J. Peardon, D. G. Richards, and C. E. Thomas, Phys. Rev. Lett. **103**, 262001 (2009), arXiv:0909.0200 [hep-ph].

[17] J. J. Dudek, R. G. Edwards, M. J. Peardon, D. G. Richards, and C. E. Thomas, Phys. Rev. D **82**, 034508 (2010), arXiv:1004.4930 [hep-ph].
[18] J. J. Dudek, R. G. Edwards, B. Joo, M. J. Peardon, D. G. Richards, and C. E. Thomas, Phys. Rev. D **83**, 111502 (2011), arXiv:1102.4299 [hep-lat].
[19] J. J. Dudek, R. G. Edwards, P. Guo, and C. E. Thomas (Hadron Spectrum), Phys. Rev. D **88**, 094505 (2013), arXiv:1309.2608 [hep-lat].
[20] T. Barnes and F. Close, Physics Letters B **123**, 89 (1983).
[21] N. Isgur and J. Paton, Physics Letters B **124**, 247 (1983).
[22] N. Isgur and J. Paton, Phys. Rev. D **31**, 2910 (1985).
[23] L. S. Kisslinger and Z. Li, Phys. Rev. D **51**, R5986 (1995).
[24] E. Golowich, E. Haqq, and G. Karl, Phys. Rev. D **28**, 160 (1983).
[25] J. J. Dudek, Phys. Rev. D **84**, 074023 (2011), arXiv:1106.5515 [hep-ph].
[26] M. Peardon, J. Bulava, J. Foley, C. Morningstar, J. Dudek, R. G. Edwards, B. Joo, H.-W. Lin, D. G. Richards, and K. J. Juge (Hadron Spectrum), Phys. Rev. D **80**, 054506 (2009), arXiv:0905.2160 [hep-lat].
[27] J. J. Dudek, R. G. Edwards, N. Mathur, and D. G. Richards, Phys. Rev. **D77**, 034501 (2008), arXiv:0707.4162 [hep-lat].
[28] H.-W. Lin et al. (Hadron Spectrum), Phys. Rev. D **79**, 034502 (2009), arXiv:0810.3588 [hep-lat].
[29] R. G. Edwards, B. Joo, and H.-W. Lin, Phys. Rev. D **78**, 054501 (2008), arXiv:0803.3960 [hep-lat].
[30] S. Borsanyi et al., JHEP **09**, 010 (2012), arXiv:1203.4469 [hep-lat].
[31] C. Morningstar and M. J. Peardon, Phys. Rev. D **69**, 054501 (2004), arXiv:hep-lat/0311018.
[32] C. J. Morningstar and M. Peardon, Phys. Rev. D **60**, 034509 (1999).
[33] R. A. Briceño and M. T. Hansen, Phys. Rev. D **92**, 074509 (2015), arXiv:1502.04314 [hep-lat].
[34] R. A. Briceño, M. T. Hansen, and A. Walker-Loud, Phys. Rev. D **91**, 034501 (2015), arXiv:1406.5965 [hep-lat].
[35] R. A. Briceño and M. T. Hansen, Phys. Rev. D **94**, 013008 (2016), arXiv:1509.08507 [hep-lat].
[36] J. Towns, T. Cockerill, M. Dahan, I. Foster, K. Gaither, A. Grimshaw, V. Hazlewood, S. Lathrop, D. Lifka, G. D. Peterson, R. Roskies, J. Scott, and N. Wilkins-Diehr, Computing in Science & Engineering **16**, 62 (2014).
[37] N. A. Nystrom, M. J. Levine, R. Z. Roskies, and J. R. Scott, in Proceedings of the 2015 XSEDE Conference: Scientific Advancements E XSEDE '15 (ACM, New York, NY, USA, 2015) pp. 30:1–30:8.
[38] R. G. Edwards and B. Joo (SciDAC, LHPC, UKQCD), Lattice field theory. Proceedings, 22nd International Symposium, Lattice 2004, Nucl. Phys. Proc. Suppl. **140**, 832 (2005), [,832(2004)], arXiv:hep-lat/0409003 [hep-lat].
[39] M. A. Clark, R. Babich, K. Barros, R. C. Brower, and C. Rebbi, Comput. Phys. Commun. **181**, 1517 (2010), arXiv:0911.3191 [hep-lat].
[40] R. Babich, M. A. Clark, and B. Joo, in SC 10 (Supercomputing 2010) (2010) arXiv:1011.0024 [hep-lat].
[41] B. Joó, D. D. Kalamkar, T. Kurth, K. Vaidyanathan, and A. Walden, in High Performance Computing: ISC High Performance 2016 International Workshops, ExaComm, E-MuCoCoS, HPC-IODC, IXPUG, edited by M. Taufer, B. Mohr, and J. M. Kunkel (Springer International Publishing, Cham, 2016) pp. 415–427.